Toward an Understanding of the Structure of Jupiter's Atmosphere Using the Ammonia Distribution and the Transformed Eulerian Mean Theory

SUKYOUNG LEE[a] AND YOHAI KASPI[b]

[a] *Department of Meteorology and Atmospheric Science, The Pennsylvania State University, University Park, Pennsylvania*
[b] *Department of Earth and Planetary Sciences, Weizmann Institute of Science, Rehovot, Israel*

(Manuscript received 14 November 2020, in final form 13 April 2021)

ABSTRACT: The structure and stability of Jupiter's atmosphere is analyzed using transformed Eulerian mean (TEM) theory. Utilizing the ammonia distribution derived from microwave radiometer measurements of the *Juno* orbiter, the latitudinal and vertical distribution of the vertical velocity in the interior of Jupiter's atmosphere is inferred. The resulting overturning circulation is then interpreted in the TEM framework to offer speculation of the vertical and meridional temperature distribution. At midlatitudes, the analyzed vertical velocity field shows Ferrel-cell-like patterns associated with each of the jets. A scaling analysis of the TEM overturning circulation equation suggests that in order for the Ferrel-cell-like patterns to be visible in the ammonia distribution, the static stability of Jupiter's weather layer should be on the order of $1 \times 10^{-2}\,s^{-1}$. At low latitudes, the ammonia distribution suggests strong upward motion, which is reminiscent of the rising branch of the Hadley cell where the static stability is weaker. Taken together, the analysis suggests that the temperature lapse rate in the midlatitudes is markedly smaller than that in the low latitudes. Because the cloud-top temperature is nearly uniform across all latitudes, the analysis suggests that in the interior of the weather layer, there could exist a temperature gradient between the low- and midlatitude regions.

KEYWORDS: Atmospheric circulation; Large-scale motions; Planetary atmospheres

1. Introduction

The Jovian alternating cloud bands and jet streams have been a subject of significant interest (Vasavada and Showman 2005; Sanchez-Lavega et al. 2019). Jupiter's fast rotation and large-scale flows make it an ideal object for studying geophysical flows and as more data are acquired the planet can be studied in more detail. A key impediment for understanding how the Jovian general circulation—most notably the extremely persistent east–west alternating multiple jets and active eddies at cloud level—arises is the lack of knowledge of its internal thermal structure. The vertical and horizontal variations of atmospheric temperature are fundamental components of the general circulation, yet it is challenging to make measurements of the vertical temperature distribution. The only in situ measurements come from the Galileo probe that provided a single in situ profile down to a level of 22 bars at 6.5° latitude in the Northern Hemisphere (Seiff et al. 1998; Atkinson et al. 1998).

In the last few years, the *Juno* orbiter has provided a wealth of information about the planet. Particularly, *Juno's* gravity and microwave measurements provided new information regarding the atmospheric structure and dynamics. The gravity measurements revealed that the strong east–west multiple jet streams penetrate deep into the planetary interior to depths of roughly 3000 km (Kaspi et al. 2018), where electric conductivity rises and possibly dampens the flows (Liu et al. 2008; Kaspi et al. 2020). The microwave measurements revealed significant variations in ammonia abundance down to a pressure of about a hundred bars (Bolton et al. 2017; Li et al. 2017; Ingersoll et al. 2017).

The goal of this study is to use the transformed Eulerian mean (TEM) framework (Andrews and McIntyre 1976) to gain insight into the Jovian atmosphere's overturning circulations by analyzing the *Juno* microwave radiometer measurements of ammonia distribution (Li et al. 2017). The TEM framework was used to gain insight into how the Earth atmosphere's midlatitude jets are maintained (Robinson 2006), and to conjecture the existence of jet-scale overturning circulations in the Southern Ocean (Li et al. 2016; Li and Lee 2017) which was later supported by observations by Argo floats (Li et al. 2018). In this study, the TEM theory is applied toward possibly understanding the internal thermal structure of Jupiter by interpreting jet-scale overturning circulations evident in the ammonia distribution. Specifically, we seek 1) to determine the structure of the overturning circulations, and by interpreting this circulation structure in the TEM framework, 2) to offer some speculation on the temperature distribution. The TEM overturning circulation is not exactly equal to zonal-mean Lagrangian motion, as pointed out by Andrews and McIntyre (1976), but as was shown in tracer transport studies (e.g., Abalos et al. 2017), the TEM equations provide useful insights into the dynamical processes that are behind the observed tracer distribution.

This paper is organized as follows: Some general features of the ammonia distribution are first described in section 2. In section 3, we offer an interpretation for how the TEM equation can be used to infer the static stability of Jupiter's atmosphere in the region where jet-scale ammonia fluctuations are observed. Using the TEM equation and the ammonia distribution, the vertical velocity field is estimated and the result is presented in section 4. Section 5 offers a discussion on the meridional temperature gradient and its implications for a

Corresponding author: Sukyoung Lee, sxl31@psu.edu

DOI: 10.1175/JAS-D-20-0342.1

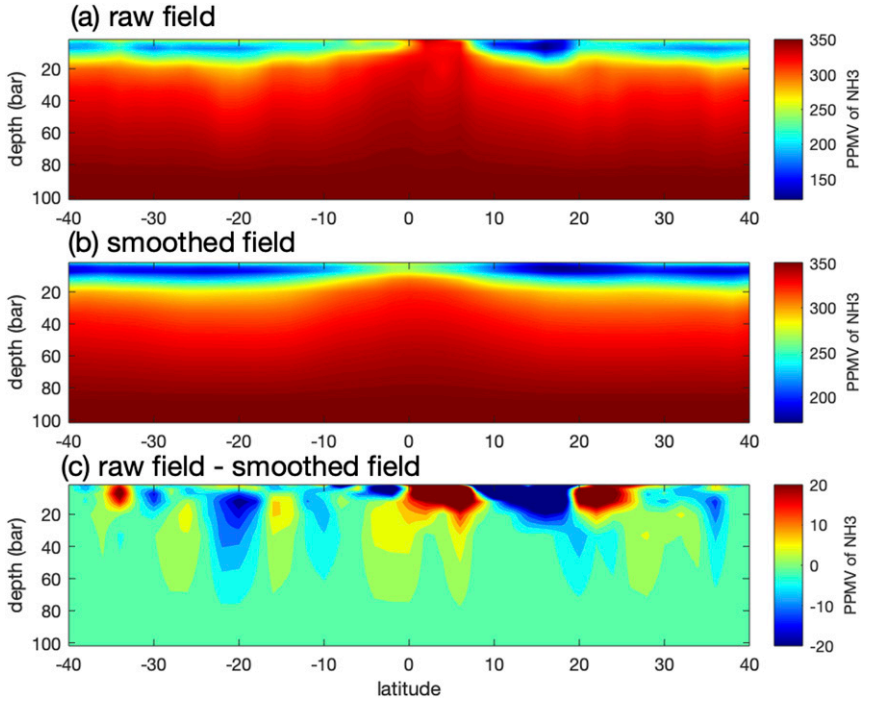

FIG. 1. (a) The observed ammonia abundance from *Juno*'s first orbit of Jupiter (Bolton et al. 2017). (b) As in (a), but using a 20° running latitudinal mean. (c) The difference between (a) and (b).

possible mechanism that could account for the maintenance of both the jets and the overturning circulations.

2. Synopsis of the ammonia distribution

The ammonia distribution derived from the *Juno* microwave radiometer measurements reveals features that suggest vertical motions (Bolton et al. 2017). This distribution, reproduced here as Fig. 1a, shows that centered at Jupiter's equator there is a pluming feature reminiscent of a deep Hadley cell. Ingersoll et al. (2017) discuss such a Hadley cell, but question its existence because of inability to close the ammonia budget. They suggest the possibility that the upwelling of ammonia observed at the equator may be balanced by downwelling at latitudes higher than 40°, which are not covered by the microwave measurements. As will be discussed later, we use TEM to consider this possibility.

Although not as striking, there are midlatitude features that also suggest substantial vertical motions. The close alignment between the zonal wind and eddy momentum flux (Salyk et al. 2006) indicates that the zonal wind is driven by meridional convergence of eddy zonal momentum as for the eddy-driven, polar-front jets of Earth's atmosphere (Ingersoll et al. 2017). Comparing the ammonia field with the zonal wind profile, shown in Fig. 3 (the vertical velocity in this figure will be discussed later), there are some hints of upward protrusions of high concentration of ammonia on the poleward flank of the westerly (i.e., eastward) jets, suggesting rising motion. On the equatorward flank of the same jets, there are hints of downward motion, as suggested by the downward intrusion of lower concentration of ammonia gas. This vertical motion distribution, relative to the jet, is consistent with the circulation model proposed by Showman and de Pater (2005), who based their model on the ground-based radio observations of Jupiter's ammonia. The ammonia data used by Showman and de Pater (2005) were limited in that unlike the *Juno* measurements, horizontal structure of the vertical distribution of the ammonia concentration was unavailable. Therefore, it is remarkable that the *Juno* measurements paint a picture consistent with the earlier work, and it is worth investigating the implied vertical motion.

The ammonia distribution is taken during the first *Juno* orbit of Jupiter (PJ1) while the zonal wind and eddy momentum flux are obtained from a zonal average, hence caution is called for when trying to synthesize these observations. At the time of this writing, ammonia retrievals for other passes are unavailable for this study. However, the latitudinal profiles of brightness temperatures from PJ1, PJ3–PJ9, and PJ12, shown in Fig. 9 of Oyafuso et al. (2020), reveal that the nine latitudinal profiles are almost indistinguishable from each other. This alignment across different longitudes is consistent with the fact that the zonal variation in the observed zonal wind is small. Because the ammonia distribution is retrieved from brightness temperatures, we believe that the PJ1 ammonia field is a reasonable representation of the zonal-mean field. In fact, comparing our Fig. 1a with Fig. 1 of Guillot et al. (2020), which displays the ammonia retrieval from PJ1 to PJ9, the latitudes of the jet-scale vertical

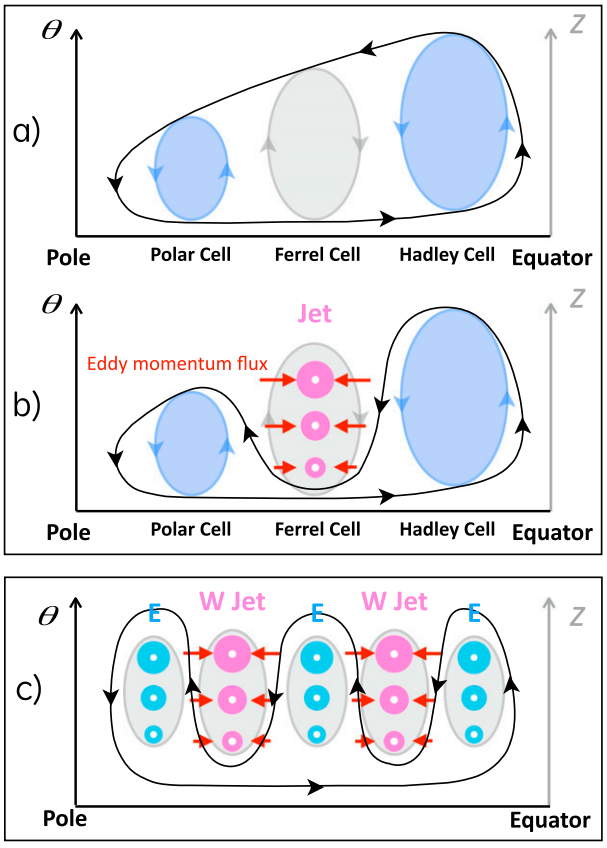

FIG. 2. Schematic diagram of both Eulerian (gray) and TEM circulations (black) for Earth. (a) The circulation driven by the eddy buoyancy flux; (b) the circulation where eddy momentum flux effect is not negligible; (c) as in (b), but with two jets. Adapted from Li et al. (2016).

intrusions align closely to each other, especially in the 7–20 bar range that we will be focusing on.

The aforementioned implied vertical motion is in a Lagrangian sense, because this vertical motion is inferred from a material distribution. Ingersoll et al. (2000) and Schneider and Liu (2009) suggested that on Jupiter there would be a series of thermally indirect cells, each associated with individual jets, just like the Ferrel cell associated with the eddy-driven jet in Earth's atmosphere and in the same sense as the circulation depicted in Fig. 2a. They suggested that these Ferrel-like cells continue down deep into the planet until the circulation is damped by magnetic Ohmic dissipation (Liu et al. 2008), in analogy to the terrestrial cells which close at the surface due to bottom drag balancing the meridional circulation. However, the circulations that they considered are Eulerian. As explained by Robinson (2006) and Li et al. (2016), while both eddy buoyancy and momentum fluxes drive Eulerian Ferrel cells, in the TEM framework, the buoyancy flux drives a circulation opposite to the Ferrel cell, and contributes to a thermally direct, hemisphere-scale circulation which is primarily driven by radiative heating (Fig. 2a). In contrast, eddy momentum flux can still drive a thermally indirect TEM circulation, imprinting on the Eulerian Ferrel cell (Fig. 2b). (Figure 2 will be discussed in more detail in section 3.) Therefore, if Ferrel-cell-like features are evident in the ammonia distribution, with rising and sinking motions on the poleward and equatorward flanks of the eastward jets, respectively, and vice versa for the westward jets, the implication is that the eddy momentum flux contribution is as important as the buoyancy flux contribution. As will be discussed in section 3, this distinction could be used to gain some insight into the thermal structure of Jupiter's atmosphere.

The aforementioned Ferrel-cell-like features are consistent with the lower cells in the vertically stacked overturning circulation picture (Ingersoll et al. 2000; Showman and de Pater 2005; Fig. 5 of Fletcher et al. 2020). The transition level is believed to be somewhere between 1 and 4 bars, in the upper troposphere. The existence of the upper cells has been inferred from cloud and temperature observations (Conrath and Pirraglia 1983; Simon-Miller et al. 2006). The idea that there are lower cells that rotate in the opposite direction relative to the upper cells is more recent; the realization that the jets are driven by eddy momentum flux convergence led to the conclusion that below the upper cells, there must be cells that rotate in the opposite direction (Fletcher et al. 2020, and references therein). Being hidden underneath the upper cells, observational evidence of these conjectured lower cells is limited (Showman and de Pater 2005). As will be described in section 4, the PJ1 ammonia distribution offers a picture that is consistent with the lower cells. In section 5, we discuss a mechanism that could account for the generation of both the upper and lower cells.

3. Consideration of the TEM theory

The TEM theory has been widely used to interpret the large-scale circulation of Earth's atmosphere (Edmon et al. 1980, and others that follow), including the interpretation of passive tracer distributions (e.g., Abalos et al. 2017). While the TEM is not equal to Lagrangian motion (e.g., Andrews and McIntyre 1976), the TEM formalism nonetheless provides important insight into average Lagrangian motion. Also, the TEM circulation is a close approximation to the meridional circulation computed in isentropic coordinates (e.g., Vallis 2006). Therefore, for the purpose of illustrating the key ideas relevant for this study, we first briefly review the standard interpretation of the observed atmospheric circulation of Earth from the perspective of the TEM equations. These equations can be written for a nonhydrostatic and fully compressible deep atmosphere (Hardiman et al. 2010). However, because the key ideas can be illustrated under the quasigeostrophic (QG) scaling of the Boussinesq equations on a beta plane, which allows for a simpler form of equations for interpretation, the equations under these assumptions are considered here. Following Vallis (2006), the equation for the TEM residual-mean meridional circulation can be written as

$$N^2\frac{\partial^2[\phi^\dagger]}{\partial y^2}+f_0^2\frac{\partial^2[\phi^\dagger]}{\partial z^2}=\underbrace{-f_0\frac{\partial}{\partial z}\frac{\partial}{\partial y}[u^*v^*]}_{A}\underbrace{+f_0\frac{\partial^2}{\partial z^2}\left[\frac{f_0}{N^2}v^*b^*\right]}_{B}+f_0\frac{\partial}{\partial z}[F]-\frac{\partial}{\partial y}[Q], \quad (1)$$

where u, v, w, b, and N are the zonal, meridional, vertical velocities, the buoyancy, and the buoyancy frequency, respectively; and $[\phi^\dagger]$ is a streamfunction that satisfies $[w^\dagger] = \partial[\phi^\dagger]/\partial y$ and $[v^\dagger] = -\partial[\phi^\dagger]/\partial z$, which is allowed from the continuity equation, $\partial[v^\dagger]/\partial y + \partial[w^\dagger]/\partial z = 0$. The square brackets $[\cdot]$ denote a zonal mean, and the asterisks denote the deviation from the zonal mean. The Coriolis parameter is denoted as f_0. F is nonconservative mechanical forcing and Q is diabatic heating. On the left-hand side of (1), the daggered velocities ($[v^\dagger]$, $[w^\dagger]$) denote the TEM residual-mean circulation. They are defined as

$$[v^\dagger] = [v] - \frac{\partial}{\partial z}\left[\frac{1}{N^2}v^*b^*\right] \quad \text{and} \quad [w^\dagger] = [w] + \frac{\partial}{\partial y}\left[\frac{1}{N^2}v^*b^*\right]. \tag{2}$$

Equation (1) is derived by combining the zonal-mean zonal momentum equation and the buoyancy equation,

$$\frac{\partial[u]}{\partial t} = f_0[v^\dagger] - \frac{\partial}{\partial y}[u^*v^*] + \frac{\partial}{\partial z}\left[\frac{f_0}{N^2}v^*b^*\right] + [F]$$

and

$$\frac{\partial[b]}{\partial t} = N^2[w^\dagger] + [Q],$$

respectively, using the requirement that the wind and buoyancy fields be maintained in thermal wind balance:

$$f_0\frac{\partial[u]}{\partial z} = -\frac{\partial[b]}{\partial y}.$$

In other words, (1) describes the overturning circulation that must arise in order to restore thermal wind balance (geostrophic and hydrostatic balance) if the balance is disturbed by the eddy momentum flux (term A) and/or the eddy buoyancy flux (term B).

In Earth's atmosphere, the eddy buoyancy flux is poleward everywhere, peaking in midlatitudes. Therefore, if the eddy buoyancy flux for Jupiter is also poleward at all latitudes, then as for Earth, term B will drive a counterclockwise TEM circulation in the Southern Hemisphere (SH), as depicted in Fig. 2a. In the Northern Hemisphere (NH), term B will drive a clockwise TEM circulation.

In a state with multiple zonal jets, in general, one may wonder if the eddy buoyancy flux is stronger at the jet latitude and weaker in the interjet regions. However, as shown using two-layer models (Lee 1997, 2005) and in an eddy-resolving ocean model (Li et al. 2016), the eddy buoyancy flux is just as strong in the interjet regions because the flow is still baroclinically unstable in the interjet regions, even when the upper-level jet is westward because the lower-level wind is more westward (e.g., see Fig. 7c of Lee 1997). In fact, the linear stability analysis shown in Lee (1997) reveals that the fastest growing baroclinic mode corresponds to interjet baroclinic waves (Fig. 8 of Lee 1997). The reason why this mode has a greater growth rate than the waves that grow in the eastward jet regions is unclear. It may be that in the interjet region, the meridional shear of the background zonal wind is weaker, and therefore the "barotropic governor" effect (James 1987) that suppresses baroclinic growth is not as strong. Therefore, we believe that the TEM circulation that results from term B is a hemisphere-scale counterclockwise circulation in the Southern Hemisphere, and clockwise circulation in the Northern Hemisphere.

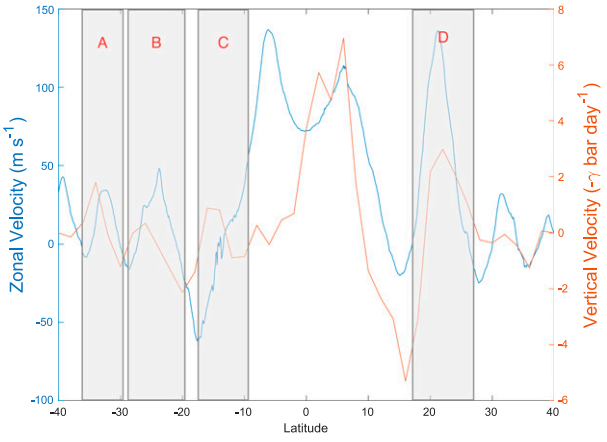

FIG. 3. The observed zonal velocity from cloud-top level (blue) and vertically averaged (7–20 bars) perturbation vertical "velocity" field $[\omega]'$computed using (7).

On Jupiter, baroclinic instability is generally expected to be weak because of the weak observed equator-to-pole temperature gradients (Fletcher et al. 2016). However, when considering that the atmosphere of Jupiter extends deep, baroclinic instability is possible (Conrath et al. 1981; Kaspi and Flierl 2007; Lian and Showman 2008). This possibility will be discussed further in section 5.

We next evaluate and compare the impact of the eddy momentum fluxes with eddy buoyancy fluxes on the residual circulation. As will be explained shortly, the eddy momentum flux contribution drives jet-scale overturning circulations (JSOCs; after Li et al. 2016) with rising motion on the poleward flank of eastward jets and sinking motion on the equatorward flank of eastward jets, as the circulation depicted in Fig. 2b. To see why this is the case, we examine Eq. (1). For the Southern Hemisphere, where $f_0 < 0$, Eq. (1) indicates that positive and negative forcings on the rhs of (1) drive clockwise and counterclockwise circulations, respectively, in the y–z plane. For the eddy-driven jet of Earth's atmosphere, the eddy momentum flux convergence in term A increases with height. Therefore, in the Southern Hemisphere, term A drives a clockwise TEM circulation centered around the eddy-driven westerly jets, as depicted in Fig. 2b. In the Northern Hemisphere, term A drives counterclockwise TEM JSOCs. In a state with multiple zonal jets where term A is comparable with term B, there would be Ferrel-cell-like JSOCs associated with each of the westerly jets (Fig. 2c). As shown in Fig. 3, poleward of ~10° latitude, Jupiter's ammonia distribution paints a picture consistent with Fig. 2c, because Ferrel-cell-like JSOCs are associated with the westerly jets. Therefore, it can be concluded that on Jupiter term A is at least comparable with term B. It is also worthwhile to comment that the structure of these JSOCs is consistent with the circulation that responds to idealized momentum forcing that mimics the eddy momentum flux convergence (Zuchowski et al. 2009).

Heating and friction can also drive a TEM residual circulation. Given that more solar radiation is absorbed in equatorial regions than in polar regions, solar heating would also contribute to a hemisphere-scale counterclockwise circulation in the Southern Hemisphere. However, there is no obvious reason why heating would generate JSOCs because, if it were, the heating on the poleward flank of the eastward jets must be greater than the heating on the equatorward flank. It is possible that condensational heating could generate such jet-scale temperature fluctuations (e.g., Thomson and McIntyre 2016). However, the circulation under consideration is the lower cells (e.g., see Fletcher et al. 2020). As will be explained in section 4, the region of our analysis is below ~7 bars where the temperature is much higher than that of the ammonia cloud level of 0.7 bars where condensation occurs.

Moreover, numerical model simulations have shown that atmospheres that are subjected to a hemispheric scale (or scales much larger than the jet scale) meridional temperature gradient can spontaneously generate multiple jets through the generation of baroclinic eddy momentum fluxes (e.g., Panetta 1993; Lee 1997, 2005; Lian and Showman 2008; Chemke and Kaspi 2015). Therefore, we assume that effect of jet-scale diabatic heating, if exists, can be neglected for the purpose of our analysis. Frictional contribution may be ignored for a gas giant. Friction at the deep magnetic-dissipation level would weaken the jet, contributing to a positive vertical shear, as does the eddy momentum flux convergence. Therefore, the frictional contribution drives meridional overturning circulations in the same sense as the eddy momentum flux convergence does (Fig. 4 of Kim and Lee 2001). Kim and Lee (2001) show that the friction contribution generates a relatively shallow circulation confined to the lower troposphere. Therefore, even if friction can contribute to the overturning circulation, it is unlikely that its effect would reach the altitudes (7–20 bars; see section 4) considered in this study.

From the analysis presented here, it can be concluded that JSOCs, such as the one depicted in Fig. 2b or Fig. 2c, would emerge if term A is strong enough to rise above the effect of term B. Using QG scaling, $u = -\partial\psi/\partial y$, $v = \partial\psi/\partial x$, and $b = f_o\partial\psi/\partial z$, where ψ is the horizontal streamfunction, the ratio of term A to term B can be scaled as $O(A)/O(B) \sim [NH/(f_oL)]^2$, where H and L are the vertical and horizontal length scales of the motion, respectively. This ratio, known as Burger number (Burger 1958), measures the scale of motion relative to the Rossby radius of deformation. As was mentioned earlier, Fig. 1c shows that the jet-scale fluctuations in ammonia concentration span mainly between 1 and 20 bars. The vertical depth bounded by the 1 bar and 20 bar surfaces is about 100 km (Seiff et al. 1998). The horizontal scale of the eddies is about 5° in latitude, which is about 6.0×10^3 km. For Jupiter, $f_o = 1.8 \times 10^{-4}\,\mathrm{s}^{-1}$. Substituting these values into the above expression, we find that $O(A)/O(B) \sim (N/0.01\,\mathrm{s}^{-1})^2$

If JSOCs are visibly apparent, as described in section 2, then $O(A)/O(B)$ ~1, and certainly cannot be smaller than 0.1 (for Earth, this ratio is 1). If so, we arrive at the conclusion that N is on the order of $1 \times 10^{-2}\,\mathrm{s}^{-1}$; even using the conservative estimate of $O(A)/O(B)$ ~0.1, N is on the order of $3 \times 10^{-3}\,\mathrm{s}^{-1}$. This range of values is of the same order of magnitude as the estimates for the regions between approximately 1–7 bar depth (synthesized by Wong et al. 2011), but to the best of our knowledge there have not been prior estimates of N for the 7–20 bar range in the midlatitudes. This analysis indicates that in the region where thermally indirect JSOCs exist, the atmosphere is stably stratified. This possibility is at odds with the standard assumption that due to Jupiter's convective nature, Jupiter's atmosphere is neutrally stratified, i.e., $N = 0$ (Sugiyama et al. 2006, 2014; Liu and Schneider 2010; Palotai et al. 2014), other than local maxima caused by condensation. Although the Galileo atmospheric probe data support a relatively stable layer (Seiff et al. 1998) at 6.5°N where the probe entered the atmosphere, that Jupiter's rotation drives slantwise convection (along the direction of the spin axis instead of radially) supports Jupiter's atmosphere being close to neutral at low latitudes (O'Neill et al. 2017).

As shown in Fig. 3, the vertical velocity profile estimated from the ammonia distribution (see section 4) indicates that equatorward of ~10° latitude, such JSOCs do not exist. The background ammonia distribution in Fig. 1b suggests that there is broad upward motion in the equatorial zone bounded by ~10° of latitude. This broad upwelling is flanked by the two very strong jets on both sides of the equator, centered at 6°–8° of latitude. This is reminiscent of the relationship between the Hadley cells and the subtropical jets in Earth's atmosphere; in each hemisphere, the Hadley cell is roughly bounded by the subtropical jet. This Hadley cell–subtropical jet relationship in Jupiter's atmosphere was also previously pointed out (Yamazaki et al. 2005). All of these considerations suggest that the static stability in the equatorial zone is much smaller than that of the extraequatorial zone.

4. Estimation of vertical motion from the ammonia distribution

The equation for zonal-mean ammonia distribution in the TEM framework may be written as

$$\frac{\partial[\chi]}{\partial t} = -[v^\dagger]\frac{\partial[\chi]}{\partial y} - [w^\dagger]\frac{\partial[\chi]}{\partial z} - \gamma[\chi], \tag{3}$$

where $[\chi]$ is zonal-mean ammonia mixing ratio and $([v^\dagger], [w^\dagger])$ are the TEM meridional and vertical velocities. The last term, $-\gamma[\chi]$, is a crude representation of the eddy flux divergence term [e.g., the last term in Eq. (9.4.13) of Andrews et al. 1987] which cannot be evaluated with currently available data. The coefficient γ is the decay rate, and may be scaled as νl^{-2} where ν is the diffusion coefficient and l is the length scale. We opted to use this linear damping form $-\gamma[\chi]$ rather than the diffusion form because it allows us to evaluate the velocity using a local value of $[\chi]$ without having to solve the equation that requires assumptions of boundary conditions, and also assumptions about the value of ν. With the understanding that γ is the decay rate, and can be scaled as νl^{-2}, we believe that the physical meaning and limitations of the analysis are more transparent to readers.

In (3), sources/sinks due to evaporation/condensation and chemical reactions are neglected. Because the base of the ammonia cloud is at 0.7 bars, we assume that the source/sink of

ammonia gas between 7 and 20 bars can also be neglected. Guillot et al. (2020) suggested a possible source of ammonia due to "mushball" formation—ammonia dissolved into liquid water forming water–ammonia hail which carries ammonia to deeper levels creating ammonia stratification. However, the parameters regarding mushball formation are not measured and are somewhat uncertain. Therefore, we do not consider this possibility in our current analysis. Even if condensation were to occur, the increase of temperature due to the latent heat release is on the order of 0.3 K, well within the uncertainty of the brightness temperature measurements.

Figure 1a shows that there are two meridional scales, one being a hemispheric scale with the broad upward bulge in the equatorial region, and the other is the much smaller jet-scale perturbations. Therefore, in order to estimate the vertical velocity associated with jet-scale perturbations, the ammonia and velocity fields are divided into a large-scale background state and a deviation from the background state:

$$[\chi] = \overline{[\chi]} + [\chi]' \quad \text{and} \quad ([v^\dagger], [w^\dagger]) = (\overline{[v^\dagger]}, \overline{[w^\dagger]}) + ([v^\dagger]', [w^\dagger]'), \tag{4}$$

where the overbar and prime represent the large-scale background state and the perturbation from the large-scale field, respectively. The $\overline{[\chi]}$ field is obtained by applying a moving average filter in the latitudinal direction with a span of 10 grid points which corresponds to a 20° latitudinal band. The resulting smoothed field, shown in Fig. 1b, captures the hemispheric-scale ammonia field. Subtracting the field shown in Fig. 1b from that shown in Fig. 1a, i.e., $[\chi] - \overline{[\chi]}$, we obtain the jet-scale perturbation field $[\chi]'$ shown in Fig. 1c.

Substituting (4) into (3) and linearizing, a perturbation ammonia concentration equation can be obtained:

$$\frac{\partial [\chi]'}{\partial t} = -\overline{[v^\dagger]}\frac{\partial [\chi]'}{\partial y} - \overline{[w^\dagger]}\frac{\partial [\chi]'}{\partial z} - [v^\dagger]'\frac{\partial \overline{[\chi]}}{\partial y} - [w^\dagger]'\frac{\partial \overline{[\chi]}}{\partial z} - \gamma[\chi]'. \tag{5}$$

Figure 1b shows that poleward of 10°N/S, $\partial\overline{[\chi]}/\partial y$ is essentially zero. Therefore, the third term on the rhs of (5) can be ignored. This term cannot be ignored in the equatorial region, but our focus is on the jet-scale overturning circulation outside of the equatorial region. Figure 1c shows that within the region where $[\chi]'$ is large, i.e., above ~20 bars, $\partial\overline{[\chi]}/\partial z$ is large. In addition, to conserve the mass, the meridional average of $[w^\dagger]$over the entire planet must be zero. Although $\overline{[w^\dagger]}$ is not the meridional average, given that it was subjected to smoothing with a 20°-latitude window, it cannot be too large. Therefore, the second term on the rhs of (5) may also be dropped. Again, because the background $\overline{[v^\dagger]}$ has a horizontal scale much greater than the scale of $[\chi]'$, if this term is dominating, then one expects to see meridional translation of the $[\chi]'$ field with time. Because the ammonia field is derived from a snapshot, it is impossible to determine whether or not such a translation occurs, but studies using data from more orbits show a similar pattern as indicated in Fig. 1a (Li et al. 2020). If we assume that Fig. 1 represents a steady state and the $-\overline{[v^\dagger]}\partial[\chi]'/\partial y$ term can be neglected compared with both $-[w^\dagger]'\partial\overline{[\chi]}/\partial z$ and $-\gamma[\chi]'$, (5) can be simplified as $0 = [w^\dagger]'\partial\overline{[\chi]}/\partial z - \gamma[\chi]'$, and $[w^\dagger]'$ can be estimated as

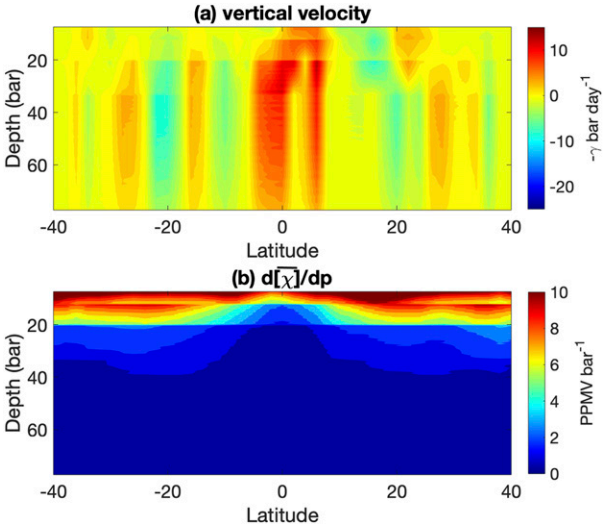

FIG. 4. (a) The perturbation vertical "velocity" field $[\omega]'$ computed using (7). (b) The vertical derivative of the background state shown in Fig. 1b.

$$[w^\dagger]' = \frac{-\gamma[\chi]'}{\dfrac{\partial\overline{[\chi]}}{\partial z}}. \tag{6}$$

Because the ammonia data are on pressure levels, we use the hydrostatic equation to express the above equation in pressure coordinates such that

$$[\omega]' = \frac{-\gamma[\chi]}{\dfrac{\partial\overline{[\chi]}}{\partial p}}, \tag{7}$$

where $\omega \equiv dP/dt$.

The value of γ is not known, but our goal is not to estimate the precise magnitude of ω', but rather to evaluate its meridional distribution. We computed ω' setting the value of γ as unity (1 day^{-1}). When the value of γ can be estimated in the future from knowledge of νl^{-2}, a quantitative value of ω' could be estimated by simply multiplying γ by the value of ω'analyzed here. For example, based on the impact comet Shoemaker–Levy 9, Friedson et al. (1999) estimated that the diffusivity of potential vorticity in Jupiter's stratosphere is approximately 3×10^5–3×10^6 m^{2}s^{-1}. Although the value of the eddy diffusivity for depths in the range of 7–20 bars is likely to be different from those in the stratosphere, if we use these values for ν and assume $l = 6.0 \times 10^3$ km, then γ is in the range of 10^{-2}–10^{-3} day^{-1}.

The resulting ω' distribution is shown in Fig. 4a. It can be seen that the velocity field is vertically aligned throughout the entire depth of the atmosphere between the top and 80 bars. This vertical alignment is consistent with prior studies that indicate that the jets extend very deep and therefore are nearly barotropic at these levels (Kaspi et al. 2018, 2020; Duer et al. 2020; Galanti and Kaspi 2021). Outside of the 20°S to 20°N region, at

most of latitudes, the estimated vertical velocity below the 20 bar level is greater than that above 20 bars. A comparison between Figs. 1c and 4b indicates that in spite of small $[\chi]'$ values, the velocity below 20 bar is large because $\partial\overline{[\chi]}/\partial p$ is dramatically smaller below that level. It is possible that this diminishingly small value of $\partial\overline{[\chi]}/\partial p$ is artificial in that spacing between the peak of the microwave channels increases. Also, above ~7 bars, the level of water condensation, $\partial\overline{[\chi]}/\partial p$ changes sign and varies rapidly (not shown). This is possibly caused by the presence of the water-cloud layers. Therefore, in the rest of the analysis, we focus on the vertical velocity averaged between 7 and 20 bars, and compare the profile with the zonal wind distribution.

Figure 3 shows that in regions A, B, and D, the vertical velocity field is consistent with the prediction of Fig. 2b (and Fig. 2c), with rising motion on the poleward flank of the eastward jets and sinking motion on the equatorward flank of the eastward jets. For region C, there is a hint of an eastward jet centered near 13°S which has the form of a shoulder of the strong equatorial jet centered at ~7°S. Salyk et al. (2006) show that there is a weak momentum flux convergence at 13°S. The absence of a clearly defined eastward jet at this latitude is due to its proximity to the much stronger jet at ~7°S. The two major jets in the equatorial zone, one centered at ~7°S and the other at ~7°N, are not accompanied by the predicted jet-scale overturning circulations, and may be related to other processes related to the formation of equatorial superrotation (Kaspi et al. 2009). Instead, in the low latitudes, there is a broad and strong rising motion, reminiscent of the Hadley circulation in Earth's atmosphere, consistent with the argument that Jupiter's equatorial zone is close to an ideal moist adiabat (Li et al. 2020).

5. Discussion and concluding remarks

From the analyses presented in this study, we draw two conclusions. First, it is likely that the jet-scale wiggly features in the ammonia field shown in Figs. 1a and 1c represent vertical motions, and that these motions are caused by eddy momentum fluxes that also drive the associated jets (Liu and Schneider 2010). These jet-scale vertical motions are likely to be embedded in a much broader hemispheric scale overturning circulation, as evidenced by the ammonia distribution (Fig. 3b). This coexistence of the two-scale overturning circulations is consistent with the theoretical expectation from TEM theory for the atmosphere with multiple eddy-momentum-driven jets (Fig. 2c).

Second, if the first conclusion is correct, we can also conclude that Jupiter's equatorial region has a relatively low static stability, as evidenced by the strong rising motion in the equatorial region, but outside of that region, the stability is markedly higher with values on the order of $1 \times 10^{-2}\,\mathrm{s}^{-1}$. It follows then that the temperature lapse rate in the equatorial region is much larger than that in the extraequatorial region where JSOCs occur. Because cloud-top temperature is almost uniform across all latitudes (Fletcher et al. 2016), the implication is that there is a temperature gradient between the low- and midlatitude regions. This gradient may be either gradual or abrupt. The latter possibility is supported by gravity measurements, which suggest that the winds are nearly barotropic, implying that the meridional temperature gradients are small in the midlatitudes (Galanti et al. 2021).

The interpretation presented in this study could provide a solution to the apparent inability of closing the ammonia budget by the Hadley-cell feature, as discussed by Ingersoll et al. (2017). As described in section 3, a poleward eddy buoyancy flux would drive hemisphere-scale overturning circulations. Latitudinally uneven radiative heating would also help drive hemisphere-scale overturning circulations. Therefore, it is plausible that the ammonia that has risen in the equatorial zone might sink back down poleward of 40° latitude, which the existing observations do not cover. It is possible that precipitation through ammonia-rich hail ("mushballs") also helps to close the budget (Guillot et al. 2020).

The vertical gradient of ammonia (Fig. 4b) is extremely small below ~20 bars. This plot indicates that the difference in ammonia concentration between 30 and 100 bars is much smaller than that between 7 and 20 bars. This vertical structure suggests that the atmosphere is stratified above ~20 bars, while it is much less so and well mixed below ~20 bars. For circulations described by an elliptic partial differential equation such as (1), the scale of the circulation can be much greater than that of the forcing. Therefore, even if forcing, such as terms A and B, is confined to above 20 bars, the vertical scale of the response can reach far below 20 bars. This vertical scale, described by the Rossby penetration depth, is inversely proportional to the static stability N. Therefore, it is plausible that below ~20 bars where N is diminishingly small, the jet signal detected by the gravity measurement may reflect the circulation response to the forcing that resides above ~20 bars, and the jets may extend very deep until the circulation closes, possibly by magnetic effects (Liu et al. 2008; Kaspi et al. 2020). This idea is consistent with the numerical model solutions presented by Showman et al. (2006) and Lian and Showman (2008).

The question then is why the region above 20 bars might be subject to baroclinic instability. Below the tropopause level, the dominant heat source of Jupiter's atmosphere is the heat from the planet's interior (Guillot 1999), but even at such a distance from the sun, the solar irradiance is not negligible (~$8\,\mathrm{W\,m}^{-2}$ on average). Due to the opacity of Jupiter's atmosphere sunlight likely does not penetrate below 20 bars or even shallower. It is plausible then that somewhere in this region of the atmosphere, the meridional gradient of the solar radiation could render the atmosphere to be baroclinically unstable. In fact, Sromovsky et al. (1996) found that solar radiation penetrates deeper than 3 bars. This equator-to-pole temperature gradient caused by solar radiation may be offset by a pole-to-equator gradient in outward internal heat flux (Kaspi et al. 2009; Brown et al. 2018). However, the finding that the energy injection scale is close to the Rossby deformation radius (Young and Read 2017) supports the possibility that baroclinic instability plays a role in exciting eddies. The solar constant of Jupiter is only 1/27 that of Earth. Therefore, if the atmosphere is baroclinically unstable, it is most likely to be less unstable than Earth's atmosphere with a smaller growth rate. In fact, idealized numerical model runs in a two-layer quasigeostrophic model show that a vertically deep and meridionally sharp jet structure, such as those on

Jupiter, is a signature of an atmosphere with weak baroclinity and weak friction (Lee 1997).

The idea that source of the eddies that drives the jets is baroclinity that resides in the relatively shallow weather layer is appealing because the resulting eddy momentum flux convergence, being present only in the shallow layer, can drive not only the lower cells that are discussed in this study, but also the upper cells just as for the stratospheric circulation of Earth's atmosphere, as described by Boehm and Lee (2003). They showed that eddy momentum flux convergence that peaks at the tropical upper troposphere can drive upwelling in the equatorial upper troposphere–lower stratosphere and downwelling directly below this upwelling. [This downwelling is not observed because it is overshadowed by the upwelling of the Hadley cell. We suggest that it is for the same reason that we see evidence of equatorial upwelling in Fig. 1, in spite of the downwelling that is predicted according to the jet-scale overturning circulation picture presented here and elsewhere (e.g., Lian and Showman 2008).] The circulation shown in Boehm and Lee (2003) is reminiscent of the vertically stacked circulation model for Jupiter's atmosphere (Showman and de Pater 2005). As reviewed by Fletcher et al. (2020), explaining this stacked circulation model remains as a challenge. Therefore, we believe that this shallow baroclinic zone idea is worth further investigation in the future.

The analysis and discussion presented here are speculative, and the title reflects this speculative nature: "Toward an understanding...." It is our hope, however, that this analysis could help design future explorations of Jupiter's atmosphere and offer a new avenue of developing models of Jupiter's atmosphere.

Acknowledgments. We thank Cheng Li for providing the *Juno* PJ1 ammonia data and for his comments on the manuscript. We are also grateful to Stephen Thomson and two anonymous reviewers for their helpful comments. SL acknowledges the facilities provided by The Pennsylvania State University for conducting this research. YK was supported by the Israeli Ministry of Science, the Minerva Foundation, and the Helen Kimmel Center for Planetary Science at the Weizmann Institute of Science.

Data availability statement. Juno MWR data can be accessed on the Planetary Data System (PDS): https://pds.nasa.gov/.

REFERENCES

Abalos, M., W. J. Randel, D. E. Kinnison, and R. R. Garcia, 2017: Using the artificial tracer e90 to examine present and future UTLS tracer transport in WACCM. *J. Atmos. Sci.*, **74**, 3383–3403, https://doi.org/10.1175/JAS-D-17-0135.1.

Andrews, D. G., and M. E. McIntyre, 1976: Planetary waves in horizontal and vertical shear: The generalized Eliassen-Palm relation and the mean zonal acceleration. *J. Atmos. Sci.*, **33**, 2031–2048, https://doi.org/10.1175/1520-0469(1976)033<2031:PWIHAV>2.0.CO;2.

——, J. R. Holton, and C. B. Leovy, 1987: *Middle Atmosphere Dynamics*. 1st ed. Academic Press, 489 pp.

Atkinson, D. H., J. B. Pollack, and A. Sei, 1998: The Galileo probe Doppler wind experiment: Measurement of the deep zonal winds on Jupiter. *J. Geophys. Res.*, **103**, 22 911–22 928, https://doi.org/10.1029/98JE00060.

Boehm, M., and S. Lee, 2003: The mechanism of tropical cirrus cloud formation and upwelling of the Brewer–Dobson circulation. *J. Atmos. Sci.*, **60**, 247–261, https://doi.org/10.1175/1520-0469(2003)060<0247:TIOTRW>2.0.CO;2.

Bolton, S. J., and Coauthors, 2017: Jupiter's interior and deep atmosphere: The initial pole-to-pole passes with the Juno spacecraft. *Science*, **356**, 821–825, https://doi.org/10.1126/science.aal2108.

Brown, S., and Coauthors, 2018: Prevalent lightning sferics at 600 megahertz near Jupiter's poles. *Nature*, **558**, 87–90, https://doi.org/10.1038/s41586-018-0156-5.

Burger, A., 1958: Scale consideration of planetary motions of the atmosphere. *Tellus*, **10**, 195–205, https://doi.org/10.3402/tellusa.v10i2.9236.

Chemke, R., and Y. Kaspi, 2015: Poleward migration of eddy-driven jets. *J. Adv. Model. Earth Syst.*, **7**, 1457–1471, https://doi.org/10.1002/2015MS000481.

Conrath, B. J., and J. A. Pirraglia, 1983: Thermal structure of Saturn from Voyager infrared measurements: Implications for atmospheric dynamics. *Icarus*, **53**, 286–292, https://doi.org/10.1016/0019-1035(83)90148-3.

——, P. J. Gierasch, and N. Nath, 1981: Stability of zonal flows on Jupiter. *Icarus*, **48**, 256–282, https://doi.org/10.1016/0019-1035(81)90108-1.

Duer, K., E. Galanti, Y. Kaspi, 2020: The range of Jupiter's flow structures that fit the Juno asymmetric gravity measurements. *J. Geophys. Res. Planets*, **125**, e2019JE006292, https://doi.org/10.1029/2019JE006292.

Edmon, H. J., Jr., B. J. Hoskins, and M. McIntyre, 1980: Eliassen-Palm cross sections for the troposphere. *J. Atmos. Sci.*, **37**, 2600–2616, https://doi.org/10.1175/1520-0469(1980)037<2600:EPCSFT>2.0.CO;2.

Fletcher, L. N., T. K. Greathouse, G. S. Orton, J. A. Sinclair, G. S. Giles, P. G. J. Irwin, and T. Encrenaz, 2016: Mid-infrared mapping of Jupiter's temperatures, aerosol opacity and chemical distributions with IRTF/TEXES. *Icarus*, **278**, 128–161, https://doi.org/10.1016/j.icarus.2016.06.008.

——, Y. Kaspi, T. Guillot, and A. Showman, 2020: How well do we understand the belt/zone circulation of giant planet atmospheres? *Space Sci. Rev.*, **216**, 30, https://doi.org/10.1007/s11214-019-0631-9.

Friedson, A. J., R. A. West, A. K. Hronek, N. A. Larsen, and N. Dalal, 1999: Transport and mixing in Jupiter's stratosphere inferred from comet S-L9 dust migration. *Icarus*, **138**, 141–156, https://doi.org/10.1006/icar.1998.6063.

Galanti, E., and Y. Kaspi, 2021: Combined magnetic and gravity measurements probe the deep zonal flows of the gas giants. *Mon. Not. Roy. Astron. Soc.*, **501**, 2352–2362, https://doi.org/10.1093/mnras/staa3722.

——, and Coauthors, 2021: Constraints on the latitudinal profile of Jupiter's deep jets. *Geophys. Res. Lett.*, **48**, e2021GL092912, https://doi.org/10.1029/2021GL092912.

Guillot, T., 1999: Interiors of giant planets inside and outside the solar system. *Science*, **286**, 72–77, https://doi.org/10.1126/science.286.5437.72.

——, and Coauthors, 2020: Storms and the depletion of ammonia in Jupiter: II. Explaining the Juno observations. *J. Geophys. Res. Planets*, **125**, e2020JE006404, https://doi.org/10.1029/2020JE006404.

Hardiman, S. C., D. G. Andrews, A. A. White, N. Butchart, and I. Edmond, 2010: Using different formulations of the transformed Eulerian mean equations and Eliassen–Palm diagnostics in general circulation models. *J. Atmos. Sci.*, **67**, 1983–1995, https://doi.org/10.1175/2010JAS3355.1.

Ingersoll, A. P., and Coauthors, 2000: Moist convection as an energy source for the large-scale motions in Jupiter's atmosphere. *Nature*, **403**, 630–632, https://doi.org/10.1038/35001021.

——, and Coauthors, 2017: Implications of the ammonia distributions on Jupiter from 1 to 100 bars as measured by the Juno microwave radiometer. *Geophys. Res. Lett.*, **44**, 7676–7685, https://doi.org/10.1002/2017GL074277.

James, I. N., 1987: Suppression of baroclinic instability in horizontally sheared flows. *J. Atmos. Sci.*, **44**, 3710–3720, https://doi.org/10.1175/1520-0469(1987)044<3710:SOBIIH>2.0.CO;2.

Kaspi, Y., and G. R. Flierl, 2007: Formation of jets by baroclinic instability on gas planet atmospheres. *J. Atmos. Sci.*, **64**, 3177–3194, https://doi.org/10.1175/JAS4009.1.

——, ——, and A. P. Showman, 2009: The deep wind structure of the giant planets: Results from an anelastic general circulation model. *Icarus*, **202**, 525–542, https://doi.org/10.1016/j.icarus.2009.03.026.

——, and Coauthors, 2018: Jupiter's atmospheric jet streams extend thousands of kilometres deep. *Nature*, **555**, 223–226, https://doi.org/10.1038/nature25793.

——, E. Galanti, A. P. Showman, D. J. Stevenson, T. Guillo, L. Iess, and S. J. Bolton, 2020: Comparison of the deep atmospheric dynamics of Jupiter and Saturn in light of the Juno and Cassini gravity measurements. *Space Sci. Rev.*, **216**, 84, https://doi.org/10.1007/s11214-020-00705-7.

Kim, H., and S. Lee, 2001: Hadley cell dynamics in a primitive equation model. Part II. Nonaxisymmetric flow. *J. Atmos. Sci.*, **58**, 2845–2858, https://doi.org/10.1175/1520-0469(2001)058<2859:HCDIAP>2.0.CO;2.

Lee, S., 1997: Maintenance of multiple jets in a baroclinic flow. *J. Atmos. Sci.*, **54**, 1726–1738, https://doi.org/10.1175/1520-0469(1997)054<1726:MOMJIA>2.0.CO;2.

——, 2005: Baroclinic multiple zonal jets on the sphere. *J. Atmos. Sci.*, **62**, 2484–2498, https://doi.org/10.1175/JAS3481.1.

Li, C., and Coauthors, 2017: The distribution of ammonia on Jupiter from a preliminary inversion of Juno microwave radiometer data. *Geophys. Res. Lett.*, **44**, 5317–5325, https://doi.org/10.1002/2017GL073159.

——, and Coauthors, 2020: The water abundance in Jupiter's equatorial zone. *Nat. Astron.*, **4**, 609–616, https://doi.org/10.1038/s41550-020-1009-3.

Li, Q., and S. Lee, 2017: A mechanism of mixed-layer formation in the Indo–western Pacific Southern Ocean: Preconditioning by an eddy-driven jet-scale overturning circulation. *J. Phys. Oceanogr.*, **47**, 2755–2772, https://doi.org/10.1175/JPO-D-17-0006.1.

——, ——, and A. Griesel, 2016: Eddy fluxes and jet-scale overturning circulations in the Indo–western Pacific Southern Ocean. *J. Phys. Oceanogr.*, **46**, 2943–2959, https://doi.org/10.1175/JPO-D-15-0241.1.

——, ——, and M. Mazloff, 2018: Evidence of jet-scale overturning ocean circulation in Argo float trajectories. *Geophys. Res. Lett.*, **45**, 11 866–11 874, https://doi.org/10.1029/2018GL078950.

Lian, Y., and A. P. Showman, 2008: Deep jets on gas-giant planets. *Icarus*, **194**, 597–615, https://doi.org/10.1016/j.icarus.2007.10.014.

Liu, J., and T. Schneider, 2010: Mechanisms of jet formation on the giant planets. *J. Atmos. Sci.*, **67**, 3652–3672, https://doi.org/10.1175/2010JAS3492.1.

——, P. Goldreich, and D. Stevenson, 2008: Constraints on deep-seated zonal winds inside Jupiter and Saturn. *Icarus*, **196**, 653–664, https://doi.org/10.1016/j.icarus.2007.11.036.

O'Neill, M. E., Y. Kaspi, and L. N. Fletcher, 2017: Galileo probe interpretation indicating a neutrally stable layer in the Jovian troposphere. *Geophys. Res. Lett.*, **44**, 4008–4017, https://doi.org/10.1002/2017GL073305.

Oyafuso, F., and Coauthors, 2020: Angular dependence and spatial distribution of Jupiter's centimeter-wave thermal emission from Juno's microwave radiometer. *Earth Space Sci.*, **7**, e2020EA001254, https://doi.org/10.1029/2020EA001254.

Palotai, C., T. E. Dowling, and L. N. Fletcher, 2014: 3D modeling of interactions between Jupiter's ammonia clouds and large anticyclones. *Icarus*, **232**, 141–156, https://doi.org/10.1016/j.icarus.2014.01.005.

Panetta, R. L., 1993: Zonal jets in wide baroclinically unstable regions: Persistence and scale selection. *J. Atmos. Sci.*, **50**, 2073–2106, https://doi.org/10.1175/1520-0469(1993)050<2073:ZJIWBU>2.0.CO;2.

Robinson, W. A., 2006: On the self-maintenance of midlatitude jets. *J. Atmos. Sci.*, **63**, 2109–2122, https://doi.org/10.1175/JAS3732.1.

Salyk, C., A. P. Intersoll, J. Lorre, A. Vasavada, and A. D. Del Genio, 2006: Interaction between eddies and mean flow in Jupiter's atmosphere: Analysis of Cassini imaging data. *Icarus*, **185**, 430–442, https://doi.org/10.1016/j.icarus.2006.08.007.

Sanchez-Lavega A., and Coauthors, 2019: Gas giants. *Zonal Jets: Phenomenology, Genesis, and Physics*, Cambridge University Press, 72–103.

Schneider, T., and J. Liu, 2009: Formation of jets and equatorial superrotation on Jupiter. *J. Atmos. Sci.*, **66**, 579–601, https://doi.org/10.1175/2008JAS2798.1.

Seiff, A., and Coauthors, 1998: Thermal structure of Jupiter's atmosphere near the edge of a 5-μm hot spot in the north equatorial belt. *J. Geophys. Res.*, **103**, 22 857–22 889, https://doi.org/10.1029/98JE01766.

Showman, A. P., and I. de Pater, 2005: Dynamical implications of Jupiter's tropospheric ammonia abundance. *Icarus*, **174**, 192–204, https://doi.org/10.1016/j.icarus.2004.10.004.

——, P. J. Gierasch, and Y. Lian, 2006: Deep zonal winds can result from shallow driving in a giant-planet atmosphere. *Icarus*, **182**, 513–526, https://doi.org/10.1016/j.icarus.2006.01.019.

Simon-Miller, A. A., B. J. Conrath, P. J. Gierasch, G. S. Orton, R. K. Achterberg, F. M. Flasar, and B. M. Fisher, 2006: Jupiter's atmospheric temperatures: From Voyager IRIS to Cassini CIRS. *Icarus*, **180**, 98–112, https://doi.org/10.1016/j.icarus.2005.07.019.

Sromovsky, L. A., and Coauthors, 1996: Solar and thermal radiation in Jupiter's atmosphere: Initial results of the Galileo probe net flux radiometer. *Science*, **272**, 851–854, https://doi.org/10.1126/science.272.5263.851.

Sugiyama, K., M. Odaka, K. Kuramoto, and Y.-Y. Hayashi, 2006: Static stability of the Jovian atmospheres estimated from moist adiabatic profiles. *Geophys. Res. Lett.*, **33**, L03201, https://doi.org/10.1029/2005GL024554.

——, N. Nakajuma, M. Odaka, K. Kuramoto, and Y.-Y. Hayashi, 2014: Numerical simulations of Jupiter's moist convection layer: Structure and dynamics in statistically steady state. *Icarus*, **229**, 71–91, https://doi.org/10.1016/j.icarus.2013.10.016.

Thomson, S. I., and M. E. McIntyre, 2016: Jupiter's unearthly jets: A new turbulent model exhibiting statistical steadiness without large-scale dissipation. *J. Atmos. Sci.*, **73**, 1119–1141, https://doi.org/10.1175/JAS-D-14-0370.1.

Vallis, G. K., 2006: *Atmospheric and Oceanic Fluid Dynamics*. Cambridge University Press, 745 pp.

Vasavada, A. R., and A. P. Showman, 2005: Jovian atmospheric dynamics: An update after Galileo and Cassini. *Rep. Prog. Phys.*, **68**, 1935–1996, https://doi.org/10.1088/0034-4885/68/8/R06.

Wong, M. H., I. de Pater, X. Asay-Davis, P. S. Marcus, and C. Y. Go, 2011: Vertical structure of Jupiter's Oval BA before and after it reddened: What changed? *Icarus*, **215**, 211–225, https://doi.org/10.1016/j.icarus.2011.06.032.

Yamazaki, Y. H., P. L. Read, and D. R. Skeet, 2005: Hadley circulations and Kelvin wave-driven equatorial jets in the atmospheres of Jupiter and Saturn. *Planet. Space Sci.*, **53**, 508–525, https://doi.org/10.1016/j.pss.2004.03.009.

Young, R., and P. Read, 2017: Forward and inverse kinetic energy cascade in Jupiter's turbulent weather layer. *Nat. Phys.*, **13**, 1135–1140, https://doi.org/10.1038/nphys4227.

Zuchowski, L. C., Y. H. Yamazaki, and P. L. Read, 2009: Modeling Jupiter's cloud bands and decks: I. Jet scale meridional. *Icarus*, **200**, 548–562, https://doi.org/10.1016/j.icarus.2008.11.024.